

# Characterizing internal macropores using cross-specimen acoustic tomography: initial two dimensional results

Christopher Sherman, Mary MacLaughlin and Curtis Link  
*Montana Tech of the University of Montana, Butte, MT, USA*

Nick Hudyma  
*University of North Florida, Jacksonville, FL, USA*

**ABSTRACT:** The engineering properties of a geologic material are greatly affected by the presence of macropores. Previous research has demonstrated that the size, location, and proximity of macropores influences both the strength and stiffness of specimens. Knowledge of the distribution of macropores in a specimen prior to testing would be useful for a number of reasons. We are developing a non-destructive method called cross-specimen acoustic tomography (CSAT) currently to determine some (or all) of the macropore characteristics for a laboratory specimen. The CSAT method uses a set of piezoelectric sensors that generate and receive high frequency acoustic waves. We measure the travel times of the acoustic waves through a specimen and then use a commercially available tomography software package to invert the data. The inverted velocity model is then used to locate the voids within the specimen. Two dimensional (cross-sectional) results from plaster specimens containing large macropores of Styrofoam show the technique is promising and worthy of further development.

## 1 INTRODUCTION

Previous research has shown that the presence of macropores (large void spaces) has a significant effect on the structural behavior of geologic materials. Prior studies have used laboratory produced brittle specimens (for example DaCosta et al. 2007), numerical modeling (Jespersen et al. 2008), and real rock specimens (for example Avar and Hudyma, 2007) in attempts to quantify the effects of large voids on engineering properties. These studies showed that at the same level of macroporosity there can be large differences in strength and stiffness. This implies that the size, shape, and location of macropores within a specimen control the engineering properties of the specimen. As such, determining the size, shape, and location of macropores in a rock specimen is important for evaluating the laboratory test results.

There are a number of common imaging techniques available to characterize the internal structure(s) within geological specimens. These techniques include X-ray computed tomography (for example Mees et al. 2003), magnetic resonance imaging (for example Chen et al. 2006), ultrasound (for example Daigle et al. 2005), and computerized axial tomography (for example Vilaclara et al. 1998). A comprehensive discussion of such techniques is beyond the scope of this paper. However it is important to note that the above techniques are medical imaging techniques which require expensive equipment utilizing highly skilled personnel for operation.

The motivation for this work is to develop a simple yet robust non-destructive method to characterize macropores within laboratory specimens prior to destructive testing. Characterizing the macropores would include quantitatively determining the size, shape, and location of macropores. The technique that is being developed has been named cross-specimen acoustic tomography (CSAT). The goal is to be able to use the CSAT method to characterize the macropores and use the information to gain an understanding of how the macropores influence the variability of the engineering properties of macroporous rock. For this initial study, we used

three plaster of Paris cylindrical specimens (15.2 cm diameter by 30.5 cm length) containing a known number and size of Styrofoam inclusions.

## 2 THEORY

Elastic wave tomography is a technique that has been used in structural and geotechnical engineering to determine the locations of inclusions and defects in materials such as concrete (Diagle et al. 2005). The underlying principle behind the tomography is that the velocity of elastic waves traveling through a material is a function of the material's elastic properties. If an object contains at least two materials with distinct elastic properties, it may be possible to detect a velocity contrast in a specimen using laboratory techniques.

The primary objective of elastic wave tomography is to determine the travel times of waves passing through an object. If the geometry for a given raypath is known, then the estimated (forward model) travel time through an object may be calculated using (1), where  $\Delta t$  is the travel time of the wave,  $l$  is the length of the raypath, and  $v$  is the average velocity along the raypath. For the case where the velocity model is discretized into many pixels, the equation may be rewritten as the sum of incremental travel times given by the ratio of  $l_i$ , the length of the raypath in the pixel, and  $v_i$ , the average velocity of the pixel.

$$\Delta t = \frac{l}{v} = \sum \frac{l_i}{v_i} \quad (1)$$

Using an assumed initial velocity model, the forward model travel times can be calculated for each of the raypaths. The forward model travel times are then compared to the actual travel times (measured through testing) to determine the error. The error is used to update the velocity model and the forward model travel times are then recalculated. Several iterations are performed until the overall error is minimized for the model. Resolution of the tomographic image is a function of the wavelength of the elastic wave and the raypath density.

## 3 METHODOLOGY

CSAT is a specific application of elastic wave tomography that uses high frequency acoustic signals as the source for waves. The technique uses an acoustic emission monitoring system ( $\mu$ SAMOS™) produced by Physical Acoustics Corporation. The following is a summary of the method, as applied to plaster laboratory specimens.

### 3.1 *Specimens*

To demonstrate the CSAT method under controlled conditions, a set of three laboratory specimens were created. The specimens are composed of plaster cylinders 15.2 cm (6 inches) in diameter and 30.5 cm (12 inches) in length. One of the specimens was solid plaster of Paris. The second specimen consisted of a plaster of Paris matrix and a single 5.1 cm (2 inch) diameter Styrofoam sphere within the specimen. The third specimen consisted of a plaster of Paris matrix with two 7.6 cm (3 inch) diameter Styrofoam spheres separated by vertical distance of approximately 5.1 cm (2 inches). The plaster cylinders were allowed to cure and were then removed from the molds. After the cylinders had dried completely, a cylindrical coordinate system was carefully drawn onto the specimen to provide reference points for the data collection.

### 3.2 *Data Collection*

The data collection for the CSAT method was conducted using a set of eight piezoelectric sensors that are able to both send and receive high frequency ( $f \approx 1.26$  Khz) acoustic signals. The

sensors are placed equidistant from each other in a predetermined horizontal plane around the specimen. The sensors must be properly coupled to the specimen in order to send and record acoustic signals reliably. This was achieved by placing a small amount of semi-adhesive grease (vacuum grease) on the recording face of the sensor and by fastening each of the sensors to the specimen with rubber bands. Figure 1 shows a typical setup for the specimen and sensors.

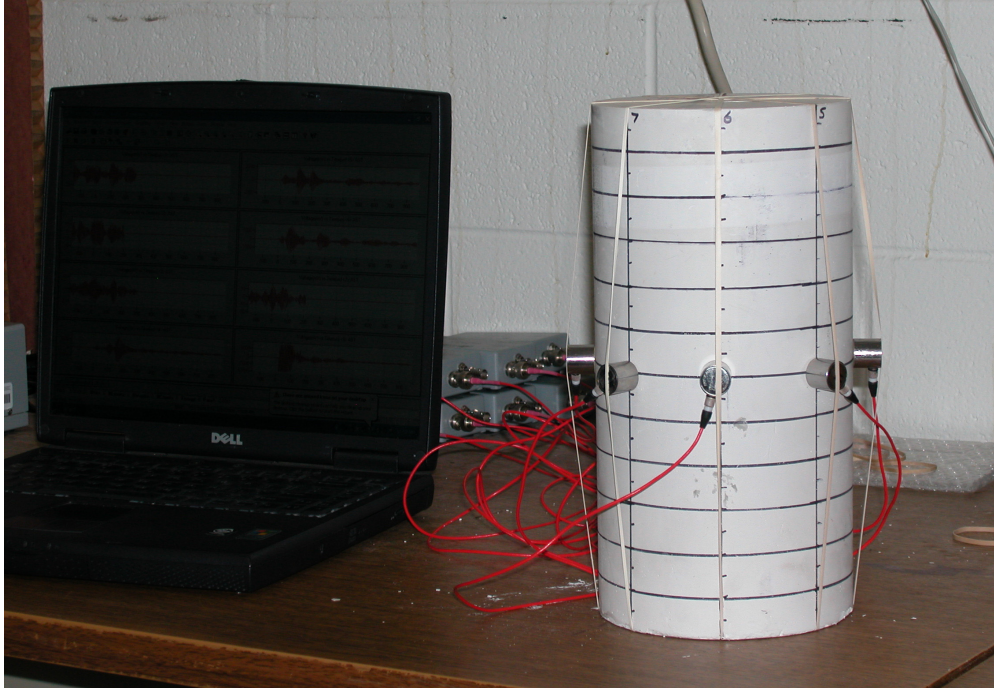


Figure 1. A typical arrangement of specimen and sensors.

After the sensors are attached to the specimen, the data collection software (AEwin) is used to trigger an Automatic Sensor Test (AST). The AST sends a  $5\mu\text{s}$  long electric signal to one sensor which creates a high frequency acoustic wave that travels through the specimen. The wave is recorded by the remaining seven sensors, and the travel times are determined. After the acoustic signal is sent and recorded, the AST waits for 100 ms and then sends another signal (PCI-8 Based AE System User's Manual, 2002). This process is repeated several times until each sensor acts as a sender ten times. Traveltimes from each test are averaged and then exported from the program as a text file.

Travel time data are recorded using an AST for a series of horizontal planes separated by 1.27 cm (0.5 inches) along the specimen's length. In order to achieve a raypath density sufficient for the data inversion, the eight sensors are rotated  $22.5^\circ$  (one-half turn) clockwise and the data are collected for the sensors in this position as well. Figure 2 shows the straight raypaths for each step of the test described above.

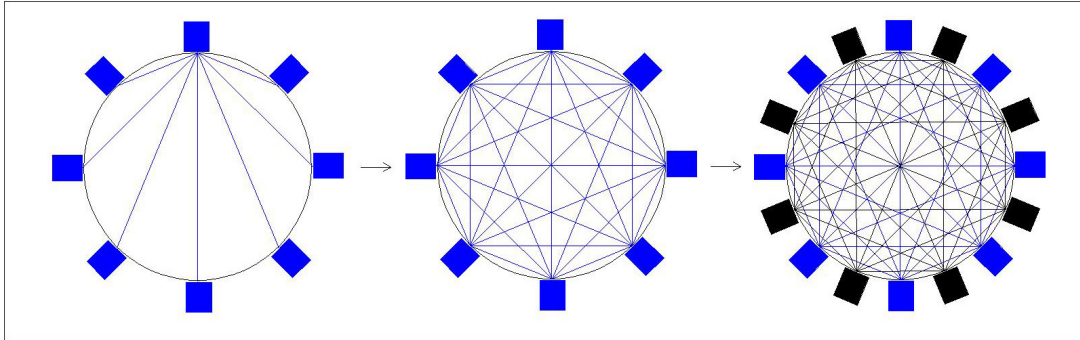


Figure 2. Straight raypaths for sensors: a) raypaths from one sensor, b) raypaths for all sensors, c) raypaths for the one-half turn configuration.

The one-half turn configuration dramatically improves raypath density. However the center of the specimen is still poorly covered by raypaths. This may lead to misinterpretation of the tomographic image, especially when attempting to detect small macropores.

### 3.3 Tomographic Inversion

The first step for the tomographic inversion is to reduce the data into appropriate form. Important information includes: the location of sources and receivers (in rectangular coordinates), travel times, and signal amplitudes (used for some inversion techniques). The data should be checked for outliers which are typically the result of hardware issues or improper sensor coupling.

Another important precursor to the data inversion is the creation of the initial velocity model. An appropriate pixel size should be chosen based upon the raypath density (it is desirable to have two or more raypaths crossing each pixel for a proper inversion). The initial velocity for each pixel should be based upon previous experience; in this case, the average velocity that was calculated for the solid plaster specimen was used.

The inversion of the data for each of the plaster cylinders was completed using the commercial software package GeoTomCG. The following is a summary of the inversion process. First, the travel time data and the initial velocity model are read by the software. Second, the number of iterations and the type of inversion are selected. Straight raypath estimations are selected for each of the data inversions. Third, the inversion is started and after several iterations a new velocity model is generated and the total error is calculated. Other useful options are available for the data inversion. These include the ability to limit the range of velocities used for the inversion, velocity damping functions, and other types of raypath estimations (Installing and Running the Three-Dimensional Tomography Program GeoTomCG, 2008).

### 3.4 Data Analysis

To analyze the inverted velocity model, it is useful to create a series of cross-sections through the specimen. It is sometimes useful to smooth the velocity model to make interpretation easier. With the contrasting elastic properties of the Styrofoam macropores compared to the plaster of Paris matrix cylinders, a velocity contrast is expected to be present in the final inverted velocity model. The location of the macropores should correspond to areas of consistent velocity contrast.

Another important parameter to consider while interpreting the results of the inversion is the root-mean-squared (RMS) error. The RMS error is calculated from the residual error (the difference between the actual and estimated travel times) for the entire velocity model. For relatively simple specimen geometries, typical RMS errors were approximately  $0.7 \mu\text{s}$ . For more complex geometries, the RMS error tends to increase by a small amount. If significant outlier

errors are present in the collected data, then the RMS tends to increase by a very large amount. It should be noted that before determining the location or size of the velocity anomalies (macro-pores), it is necessary to identify potential artifacts of the inversion process, some of which are discussed below.

#### 4 SOURCES OF ERROR

One of the largest sources of error associated with the CSAT method is due to the improper placement of sensors. To quantify the effect of small variations between the assumed locations and actual locations of the sensors, geometric relationships were used to derive a relationship for the discrepancy in the raypath lengths. This in turn may be used to determine the travel time error. The error due to the improper placement of a sensor, assuming that the velocity,  $v$ , is constant throughout the specimen, may be calculated by (2), where  $d$  is the diameter of the specimen,  $\alpha$  is the recorded angle between sensors,  $\beta$  is the actual angle between sensors (see Fig. 3),  $z$  is the difference in the elevation of the two sensors, and  $\Delta t$  is the error in the travel time.

$$\Delta t = \frac{\sqrt{\frac{d^2}{2}(1 - \cos \beta) + z^2} - \sqrt{\frac{d^2}{2}(1 - \cos \alpha)}}{v} \quad (2)$$

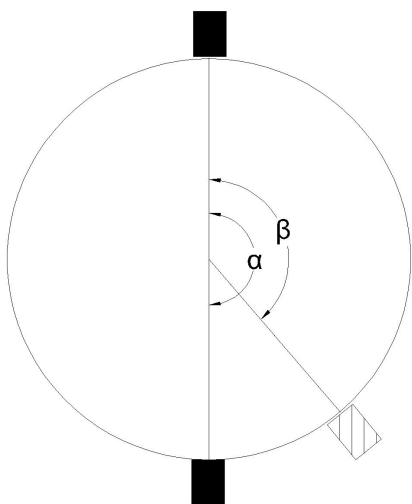


Figure 3. An illustration showing the error due between the recorded angle,  $\alpha$ , and the actual angle,  $\beta$ , between the receiving and recording sensors.

The error due to misplacement for sensors with  $\alpha$  values approaching  $180^\circ$  tend to be very small ( $<1\%$  for the width of the sensor, 1.27 cm). However, as  $\alpha$  values become smaller, the error increases significantly (up to about 20% for errors the width of the sensor). It should be noted that because the sensors used in the CSAT method have finite dimensions (e.g. are not point sources, as is assumed in the inversion) some of this error is unavoidable.

Figure 4 demonstrates the effect of sensor placement error in the collected data for a solid plaster specimen. Note that there is a zone up to about three pixels wide on the edge of the velocity model where the inverted velocity becomes highly erratic in comparison to the center pixels. This “onion skin” pattern is attributed to sensor placement error because the apparent variations in velocity appear to be random and tend to change sign near the position of a sensor. Also, if these variations were due to an actual change in acoustic wave velocity, the “onion skin” zone would tend to be symmetric about the axis of the cylinder, which it is not.

The other major source of error for this method is due to equipment, software, and/or sensor coupling issues. These errors tend to create outliers in the data sets used for the inversion. For instance, the poor coupling of a sensor may result in a set of low or high travel times for that particular sensor. If these data are included in the inversion, a pattern similar to the spokes on a wheel may appear in the velocity model. An example of this error, with unreasonably low velocity (large travel time) for one sensor is shown in Figure 5.

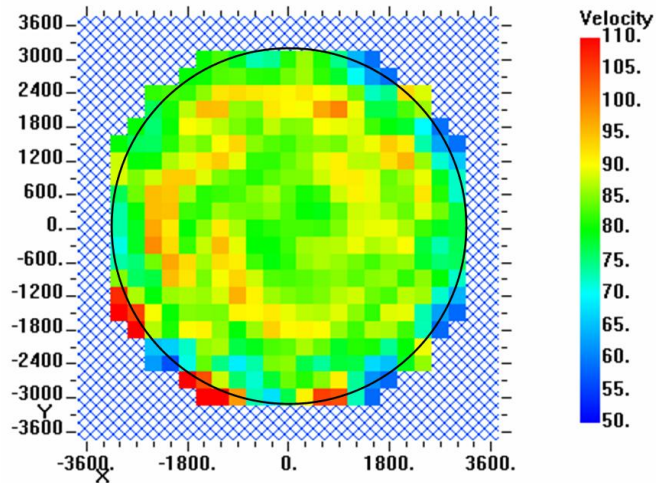


Figure 4. An “onion skin” pattern that is the result of sensor placement error.

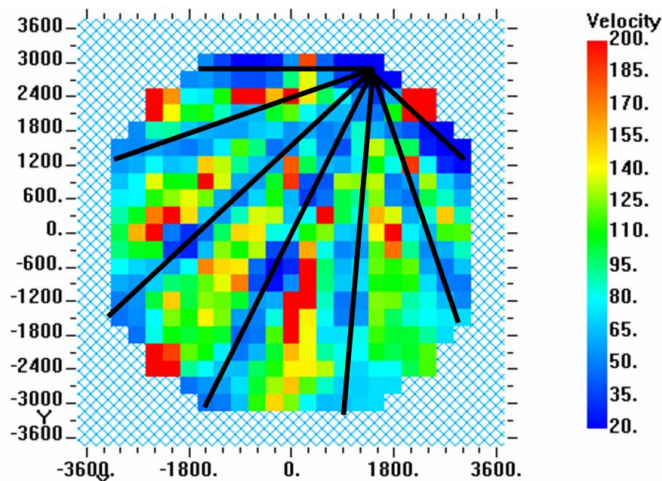


Figure 5. A radial pattern that is the result of outlier errors in the data.

## 5 RESULTS

For this initial phase of the study, the results of the CSAT characterization are horizontal tomograms (horizontal cross sections) showing pixels of computed velocities. The average velocity for solid plaster of Paris specimen is approximately 2.18 m/ms (86 in/ms). The first objective of the CSAT characterization is to determine the absolute location of the Styrofoam macropores within the specimen, which is accomplished using the series of tomograms generated by the inversion. It is important to note that only the location of the macropores is presented in the fol-

lowing section. The determination of macropore size from the tomograms is presently being investigated. The results from the two specimens are discussed below.

### 5.1 Specimen Containing a Single Macropore

The first specimen characterized contained a single spherical Styrofoam macropore that was 5.1 cm (2 inches) in diameter. The location of the macropore within the specimen was initially unknown. Horizontal tomograms were produced along horizontal planes every 1.27 cm (0.5 inches) along the height of the specimen.

In this initial study, the location of the macropores is determined by visually inspecting the tomograms and noting locations of velocity contrasts within the tomograms. The tomogram velocities are in unit of inches/ms. Based on data from the solid specimen, the macropore should be located within a low velocity zone at velocities less than 2.18 m/ms (86 in/ms), which corresponds to a color scale of light green trending to blue.

The spherical (circular in two dimensions) macropore is clearly visible tomograms B, C and D shown in Figure 6. Figure 6 contains five tomograms; three from locations for the macropore and two from locations without the macropore. Tomograms at locations B, C, D clearly show high velocity materials surrounding a lower velocity material in the center of the tomograms, which is the location of the macropore. Tomograms at locations A and E, which are at the ends of the specimen, do not show high velocity zones surrounding low velocity zones.

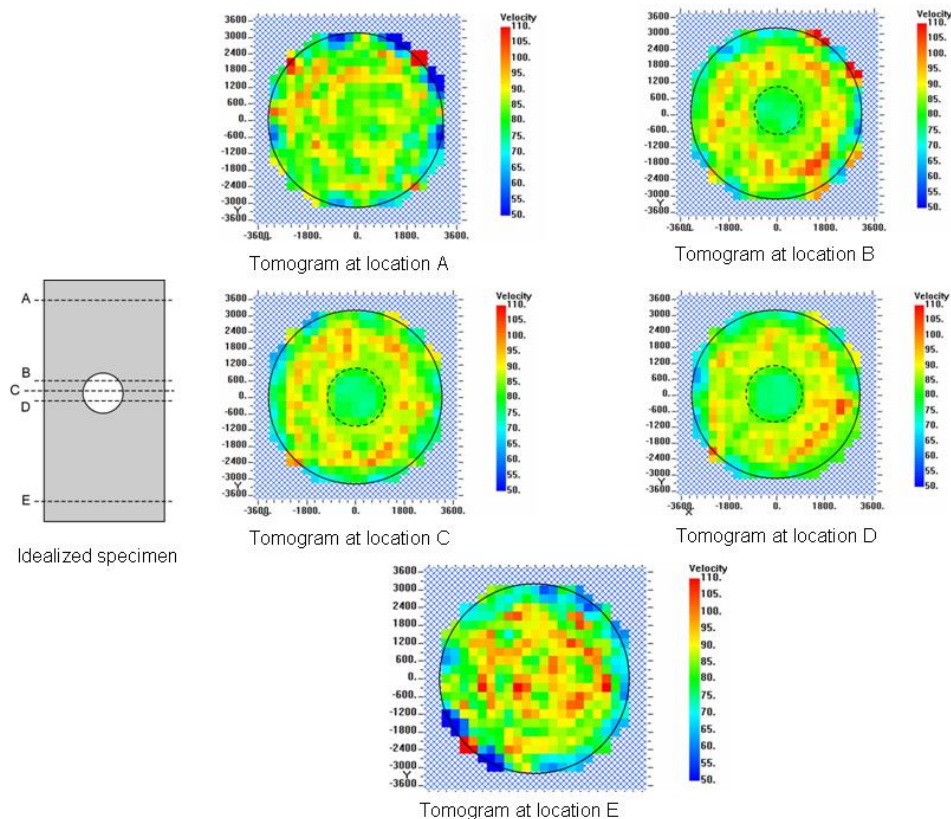


Figure 6. Two dimensional tomograms of the one macropore specimen. The dashed lines in the tomograms indicate the location of the macropore.

5.2 Specimen Containing Two Macropores

The second specimen characterized contained two 7.6 cm (3 inch) diameter spherical Styrofoam macropores. Once again the macropore locations are identified by visually locating zones of velocity contrasts within the tomograms. Figure 7 contains four tomograms; two from each of the locations of the macropores. Tomograms A and B are from the upper macropore and tomograms C and D are from the lower macropore. The locations of the macropores are easily identified by the areas of consistent velocity contrasts. This specimen has higher plaster velocities than the specimen containing the single macropore which makes macropore identification easier.

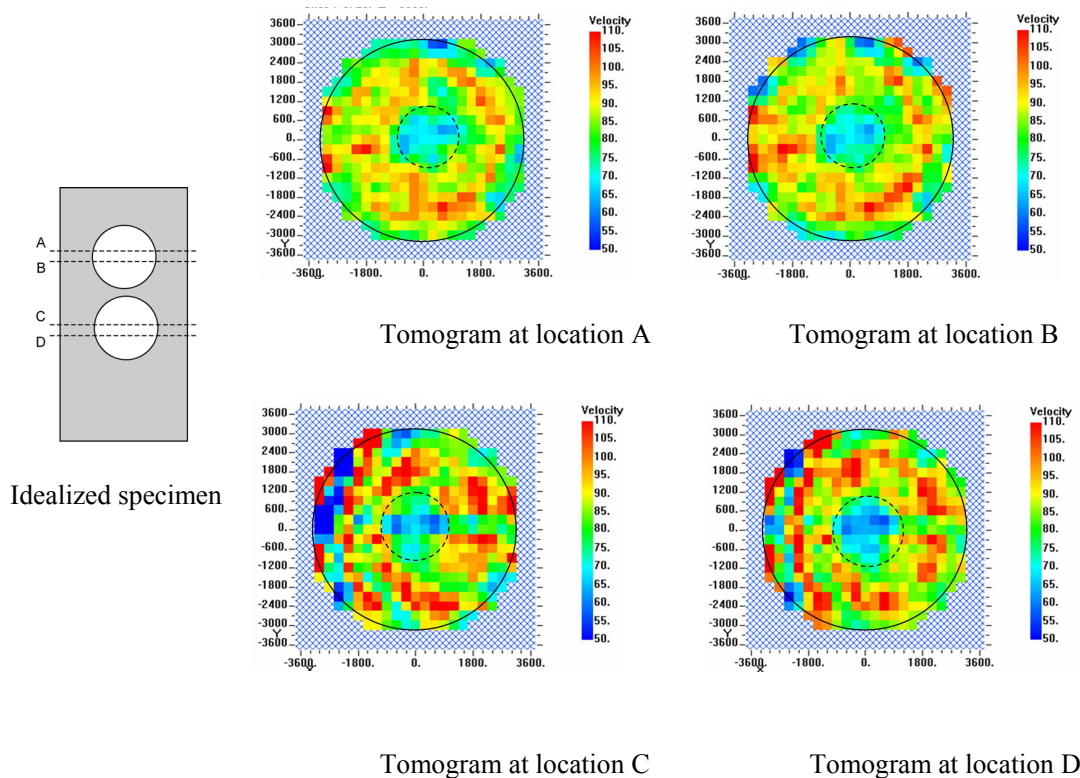


Figure 7. Two dimensional tomograms of the two macropore specimen. The dashed lines in the tomograms indicate the location of the macropores.

6 CONCLUSIONS AND FUTURE WORK

This preliminary study using cross-specimen acoustic tomography (CSAT) successfully demonstrated that acoustic wave tomography can be an effective non-destructive technique for determining the location of macropores. In order to fully develop the CSAT method into a simple yet robust method to fully characterize internal macropores, additional studies are required.

These studies will focus on additional techniques for inverting the travel time data, such as curved raypath approximations, wavefront approximations and the application of velocity damping functions. Additional improvements will include moving from two dimensional analyses to quasi-three dimensional and full three dimensional analyses.

Once a fully three-dimensional analysis is developed, the validity of the CSAT method can be assessed by dissecting specimens to determine the sizes and locations of the macropores within the specimen. Plans are currently in development to compare the CSAT results with traditional medical imaging techniques.

## ACKNOWLEDGMENTS

The research presented in this paper is supported by the National Science Foundation under Grant No. CMMI-0555812. Material costs, experimental work, and other related expenses were funded by the Montana Tech Undergraduate Research Program. The acoustic emissions equipment and software packages used in this research were supplied from the University of North Florida.

## REFERENCES

- Avar, B. and Hudyma, N., 2006. A modeling attempt to determine the relationship between porosity and deformation modulus of tuff containing cavities. In P. Lighthall (ed.) *59<sup>th</sup> Canadian Geotechnical Conference*, October 1-4, 2006, Vancouver BC, Canada, pp. 510-514
- Chen, Q., Rack, F.R. & Balcom, B.J. 2006. Quantitative magnetic resonance imaging methods for core analysis. In R.G. Rothwell (ed.) *New techniques in sediment core analysis*, Geological Society Special Publications, vol. 267, pp. 193-207, London: The Geological Society.
- DaCosta, A., Wright, C., Ye, Y., MacLaughlin, M., and Hudyma, N., 2007. Development of upper and lower bounds to describe engineering properties as a function of macroporosity. In E. Eberhardt, D. Stead, and T. Morrison (eds) *Rock Mechanics: Meeting Society's Challenges and Demands*, proceedings of the 1<sup>st</sup> Canada-US Rock Mechanics Symposium, May 27-31, 2007, Vancouver, Canada, pp. 821-826
- Daigle, M., Fratta, D. & Wang, L.B. 2005. Ultrasonic and X-ray tomographic imaging of highly contrasting inclusions in concrete specimens. In *GeoFrontier 2005 Conference*. Austin, TX
- Installing and Running the Three-Dimensional Tomography Program GeoTomCG, 2008. GeoTom, LLC, Apple Valley, MN.
- Jespersen, C., Spence, R., MacLaughlin, M., Parkhurst, J., and Hudyma, N., 2008. Strength and failure modes of macroporous rock: results from laboratory testing and 3D numerical models. *CD-ROM Proceedings of the 42nd U.S. Rock Mechanics Symposium*, San Francisco, California, Paper 08-318.
- Mees, F., Swennen, R., Van Geet, M. & Jacobs, P. 2003. Applications of X-ray computed tomography in the geosciences. In F. Mees, R. Swennen, M. Van Geet, & P. Jacobs (eds), *Applications of X-ray Computed Tomography in the Geosciences*, Geological Society Special Publications, vol. 215, pp. 1-6, London: The Geological Society.
- PCI-8 Based AE System User's Manual, Rev 0, 2002. Physical Acoustics Corporation, Princeton Junction, NJ
- Vilaclara, G., Miranda, J., Martinez-Mekler, G., Cuna, E., Rodriguez-Ramirez, A. & Zentena, M.A. 1998. Computerized axial tomography; standardization of a quick technique for lamination characterization in diatomaceous sediments. In *AMQUA 1998, American Quaternary Association program and abstracts of the 15<sup>th</sup> biennial meeting*. Volume 15, pp. 175.